Nonideal gas flow and heat transfer in micro- and nanochannels using the direct simulation Monte Carlo method

Moran Wang* and Zhixin Li
Department of Engineering Mechanics, Tsinghua University, Beijing 100084, People's Republic of China
(Received 10 March 2003; published 14 October 2003)

Subsonic nonideal gas flow and heat transfer in micro- and nanochannels for different Knudsen numbers are investigated numerically using the direct simulation Monte Carlo method modified with a consistent Boltzmann algorithm. The van der Waals equation is used as the equation of state. The collision rate is also modified based on the Enskog theory for dense gas. It is shown that the nonideal gas effect becomes significant when the gas becomes so dense that the ideal gas assumption breaks down. The results also show that the nonideal gas effect is dependent not only on the gas density, but also on the channel size. A higher gas density and a smaller channel size lead to a more significant nonideal gas effect. The nonideal gas effect also causes lower skin friction coefficients and different heat transfer flux distributions at the wall surface. The simulations presented in this work are helpful for a better understanding of micro- and nanoscale gas flows.

DOI: 10.1103/PhysRevE.68.046704 PACS number(s): 47.11.+j, 47.60.+i, 47.90.+a

I. INTRODUCTION

For gas flow in micro- and nanoscale channels, the Knudsen number can be quite high due to the small characteristic length, even though the gas density is very high indeed [1,2]. The continuum assumption then breaks down and the atomic-based methods should be used for predictions. The direct simulation Monte Carlo (DSMC) method is a particle-based numerical scheme for solving the nonlinear Boltzmann equation [3]. It has been successfully applied for rarefied gas flow simulations [4,5]. And more recently, DSMC has been used for simulating gas flows in microchannels [6–10].

In most of the previous works mentioned above, the variable hard sphere (VHS) model was used, in which the attractive potential was ignored and the gas was treated as ideal gas. However, it was found that there was no difference for velocity and temperature fields between different scales in the VHS model under the same boundary condition [11]. Although the generalized hard sphere (GHS) model [12] and the generalized soft sphere (GSS) model [13] considered the attractive potential, a new investigation showed that when gas flowed at the same Knudsen number and under the same boundary condition, little difference for simulated velocity and temperature fields between different scales could be found using different models [14], including VHS, VSS (variable soft sphere), GHS, and GSS models. All the results suggest that the micro- and nanoscale gas flows are similar to rarefied gas flows. However, as is known, though the Knudsen number in micro- and nanoscale flow may be the same as the rarefied flow, the gas can be so dense that the ideal-gas assumption may break down. Because the van der Waals equation can approximately capture slight deviations from nonideal behavior, it has been used in this exploratory study.

Theoretically, the DSMC method is restricted to dilute gas since it gives the equation of state (EOS) for a gas to the lowest order in the density. However, it is also noticed that both DSMC and the Boltzmann equation are inconsistent since the collision rate and transport properties are functions of the particle cross section while the EOS is not. This may be the reason why the DSMC cannot simulate the dense effect of gas flow, where the van der Waals force is important. A consistent Boltzmann algorithm was proposed by Alexander *et al.* [15], in which the van der Waals equation was introduced as the EOS. The consistent Boltzmann algorithm (CBA) modifications of DSMC have been used for simulation of nuclear flow [16] and surface properties of a van der Waals fluid [17]. In the present paper, the gas flow and heat transfer in micro- and nanoscale channels are investigated using a DSMC code modified with the CBA. The characteristics of fluid flow and heat transfer for different channel sizes and different Knudsen numbers are examined.

II. NUMERICAL METHOD

A. DSMC

DSMC is a molecule-based statistical simulation method for rarefied gas flow introduced by Bird. It is a numerical solution method to solve the dynamic equations for gas flow by at least thousands of simulated molecules. Each simulated molecule represents a large number of real molecules. Under the assumption of molecular chaos and gas rarefaction, the binary collisions are only considered. Therefore, the molecules' motion and their collisions are uncoupling if the computational time step is smaller than the physical collision time. The molecules' motion, interactions with boundaries, and interactions with each other are calculated, while the momentum and energy conservations are kept. The macroscopic flow characteristics are obtained statistically by sampling molecular properties in each cell.

B. CBA

The consistent Boltzmann algorithm (CBA), first introduced in 1995 [15] and developed in 1997 [18] and 2000 [17], has extended the DSMC method to a van der Waals fluid. In the CBA, a weak and constant potential to the hard core is considered due to the van der Waals EOS. The manner in the advection process in the CBA is modified to give the van der Waals EOS described below.

*Email address: moralwang99@mails.tsinghua.edu.cn

The pressure in a fluid of van der Waals particles (hard spheres with a weak, long-ranged attraction) of mass m at temperature T and number density n is given by the virial theorem as

$$P = nkT + \tfrac{1}{3} m\Gamma\Theta, \tag{1}$$

where $\Theta \equiv \langle \Delta v_{ij} \cdot r_{ij} \rangle$ is the projection of the velocity change onto the line connecting centers of particles i and j averaged over collisions (indicated by the angular brackets) and Γ is the collision rate per unit time and volume. In DSMC the second term on the right side of Eq. (1) vanishes because the positions of colliding particles are uncorrelated with the change in their velocities.

For a gas of hard spheres with diameter σ, the CBA introduces a correlation in Θ by displacing the particles in the advection step by $\boldsymbol{d}_{HS} = \sigma \hat{d}$, where the unit vector $\hat{d}$ is

$$\hat{d} = \frac{(v_i' - v_j') - (v_i - v_j)}{|(v_i' - v_j') - (v_i - v_j)|} = \frac{\boldsymbol{v}_r' - \boldsymbol{v}_r}{|\boldsymbol{v}_r' - \boldsymbol{v}_r|}, \tag{2}$$

where $\boldsymbol{v}_r$ is the relative velocity of the colliding particles, and primed and unprimed indicate post- and precollision values, respectively. After the collision, the particles are advected as

$$\boldsymbol{r}_i(t + \Delta t) = \boldsymbol{r}_i(t) + \boldsymbol{v}_i'(t)\Delta t + \boldsymbol{d}_{HS}, \tag{3}$$

$$\boldsymbol{r}_j(t + \Delta t) = \boldsymbol{r}_j(t) + \boldsymbol{v}_j'(t)\Delta t - \boldsymbol{d}_{HS}. \tag{4}$$

Equation (2) leads to an average virial $\Theta = \sigma\sqrt{\pi kT/m}$, so that using the Boltzmann (dilute gas) collision rate, $\Gamma_B = 2\sigma^2 n^2 \sqrt{\pi kT/m}$, the consistent pressure is now $P = nkT(1 + b_2 n)$, where $b_2 = \frac{2}{3}\pi\sigma^3$ is the second virial coefficient. Introducing the Enskog Y factor, which corrects the low-density collision rate to the correct hard-sphere collision rate at any density [$\Gamma_{HS} = Y(n)\Gamma_B$], into the CBA gives the correct EOS at all densities and transport coefficients at high densities corresponding to an uncorrelated collision (Markov) approximation.

The CBA is generalized to yield the van der Waals EOS by changing the advection displacement to account for the attractive force. The direction $\hat{d}$ cannot be modified without violating detailed balance, however the magnitude, which is constant for the hard-sphere model, can be made a function of density and temperature. Specifically, one obtains the van der Waals EOS,

$$\frac{P_{vdW}}{nkT} = 1 + b_2 nY - \frac{an}{kT}, \tag{5}$$

where a is the strength of the attraction. A comparison between Eq. (5) and the classical thermodynamics gives

$$a = \frac{27}{64}\frac{R^2 T_c^2}{P_c} m^2, \tag{6}$$

where R denotes the gas constant, T_c the critical temperature, P_c the critical pressure, and m the gas molecular mass [19]. The magnitude of the displacement is

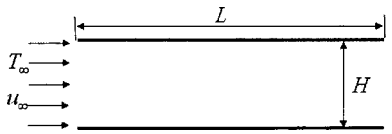

FIG. 1. Schematic of the physical problem.

$$d_{vdW} = \sigma - \frac{a\sigma}{b_2 YkT} = d_{HS} - d_a. \tag{7}$$

C. Determination of the *Y* factor

Based on the Enskog equation for dense gases [20], when a gas is so dense that the covolume of the molecules is comparable with the total volume of the system, the molecules can no longer be treated as point particles. Therefore, the common position of two colliding molecules in the Boltzmann equation should be replaced by the actual positions of the centers of two tangent spheres, and the collision frequency is influenced by correlational effects that depend on the density at the point of contact.

Due to the reduced volume occupied by the molecules, a modified higher scattering probability is

$$\Gamma' = \frac{V}{V'}\Gamma_B, \tag{8}$$

where $V' = (1 - n \cdot \frac{4}{3}\pi\sigma^3)$. However, the scattering probability is lowered again by another effect, namely that the particles are screening each other. A particle might not be available for scattering with another particle because there might be a third particle in between. This effect leads to a reduction of the scattering probability by a factor of $(1 - n\,\frac{11}{12}\,\pi\sigma^3)$. Including this factor, the modified scattering probability is

$$\Gamma_{HS} = Y(n)\Gamma_B, \tag{9}$$

where

$$Y(n) = \frac{1 - n \cdot \frac{11}{12}\pi\sigma^3}{1 - n \cdot \frac{4}{3}\pi\sigma^3} = \frac{1 - 11nb_2/8}{1 - 2nb_2} \quad \text{and} \quad b_2 = \tfrac{2}{3}\pi\sigma^3.$$

This result can, however, be trusted only to the early orders in n, since four-particle configurations have not been considered. In the current study, the expression up to third order has been used [20],

$$Y(n) = 1 + 0.625nb_2 + 0.2869(nb_2)^2 + 0.1103(nb_2)^3. \tag{10}$$

III. RESULTS AND DISCUSSION

The standard DSMC code is modified based on the CBA, with which the channel flows are simulated. The schematic of the channel flow is shown in Fig. 1. The aspect ratio L/H is set at 5.0 for all simulated cases and uniform rectangular cells (100×60) are used. The freestream velocity u_∞ and temperature T_∞ are imposed as the boundary conditions at

TABLE I. Studied cases.

Cases	L (μm)	H (μm)	Kn	u_∞ (m/s)	T_∞ (K)	n_∞	N_{total}	N_{sample}
1	5	1	1.0	200	300	1.29×10^{24}	101509	4460050
2	5	1	0.05	200	300	2.59×10^{25}	57042	500000
3	0.5	0.1	1.0	200	300	1.29×10^{25}	54229	500000
4	0.5	0.1	0.05	200	300	2.59×10^{26}	57117	301050
5	0.05	0.01	1.0	200	300	1.29×10^{26}	101355	326050
6	0.05	0.01	0.05	200	300	2.59×10^{27}	99687	257050

the inlet. The temperature at both walls is kept the same as the freestream temperature. The working fluid is nitrogen gas, whose properties are presented elsewhere [3,19]. Six cases, listed in Table I, have been simulated at fixed Knudsen numbers by decreasing the characteristic length and increasing the gas density at the same time. In the selected cases, the gas transport coefficients are little affected by the introduction of the van der Waals equation, and the values remain close to the actual values for hard spheres [21]. The results obtained using the ideal and the nonideal gas models are presented in Figs. 2–4.

A. Velocity and temperature distributions

Based on the DSMC theory, the macroscopic velocity can be obtained by the statistic laws,

$$u_j=\frac{1}{N_j}\sum u. \tag{11}$$

For a diatomic gas, the Larsen-Borgnakke model with discrete rotational energy is used to model the energy exchange between the translational and internal modes. The vibrational energy is negligible. Therefore, the temperature can be obtained as

$$T=(3T_{tr}+\zeta T_{rot})/(3+\zeta), \tag{12}$$

where T_{tr} denotes the translational temperature, T_{rot} denotes the rotational temperature, and ζ is the number of internal degree of freedom. Both T_{tr} and T_{rot} are defined as

$$\tfrac{3}{2}kT_{tr}=\overline{m\mathbf{v}^2}-\overline{m}\cdot\overline{\mathbf{v}}^2, \tag{13}$$

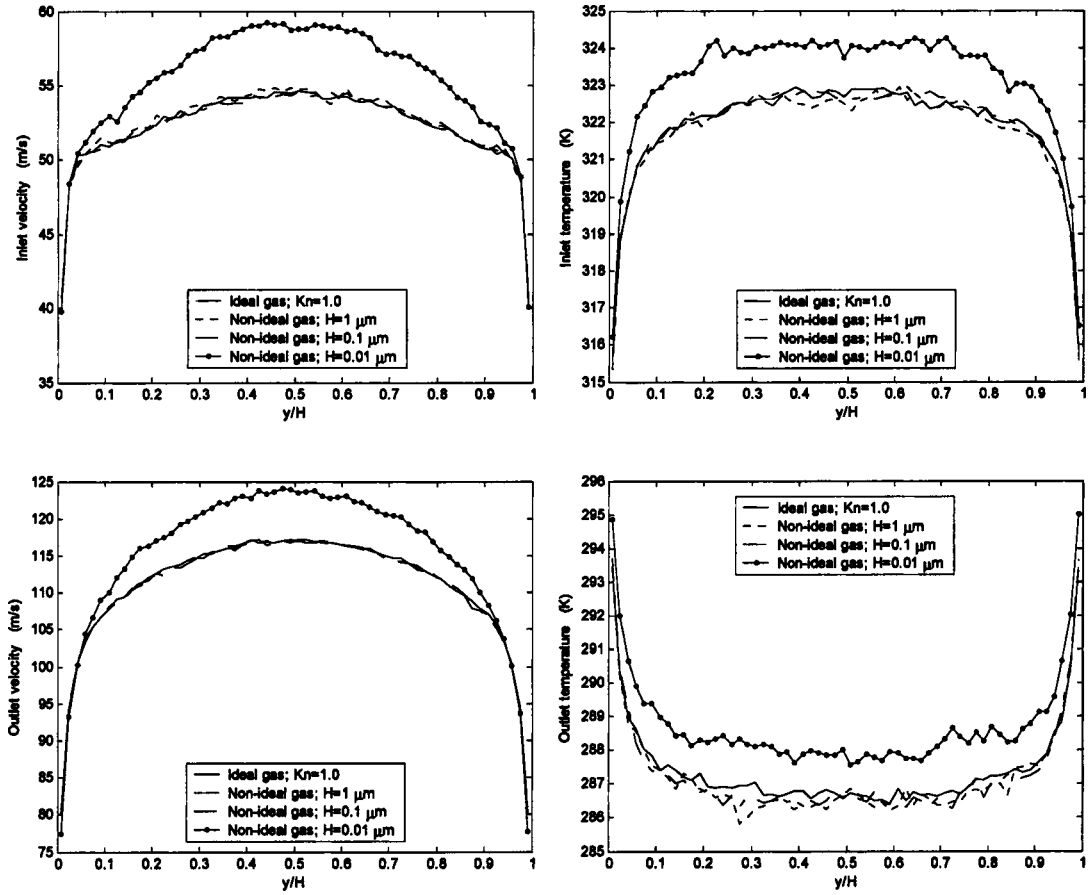

FIG. 2. Velocity and temperature distributions at the inlet and the outlet for different channel sizes at Kn=1.0.

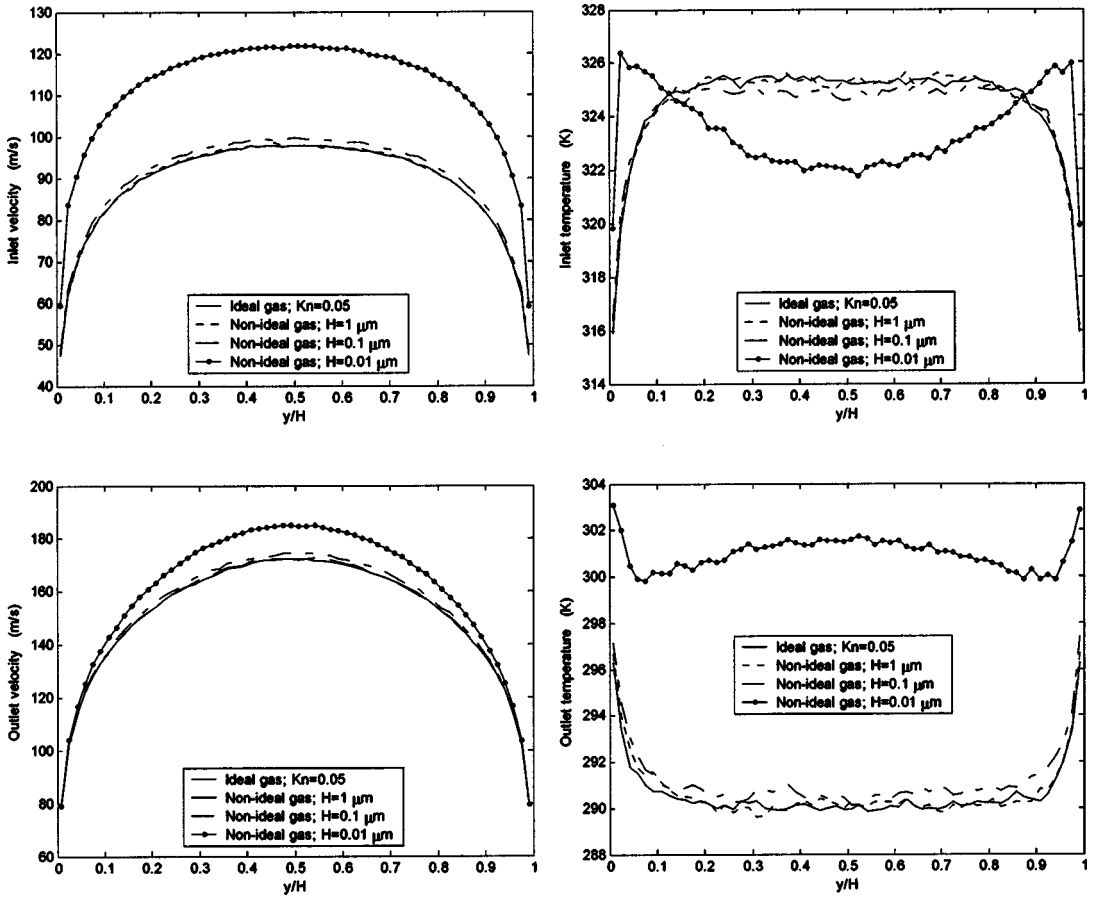

FIG. 3. Velocity and temperature distributions at the inlet and the outlet for different channel sizes at Kn=0.05.

$$T_{rot}=\frac{2}{k}(\overline{\varepsilon_{rot}/\zeta}), \tag{14}$$

where k is the Boltzmann constant, **v** is the velocity of molecules, and ε_{rot} is the rotational energy of an individual molecule.

Figure 2 shows the velocity and temperature distributions at both the inlet and outlet for different channel sizes at Kn =1.0. According to Ref. [11], when the gas is treated as ideal gas, the distributions at different scales are consistent. In Fig. 2, the solid lines represent the distributions under ideal-gas treatment. The results obtained using the nonideal-gas model for the channels having a height of 1, 0.1, and 0.01 μm are represented with dotted, dash-dot, and dashed lines, respectively. It is interesting to see from Fig. 2 that the results obtained by the ideal-gas and the nonideal-gas models for the channels having a height of 1 and 0.1 μm (case 1 and case 3) are almost identical. It should be pointed out that the fluctuations come from the statistical error. It is noticed that in both cases the density is so low that the rarefied gas assump-

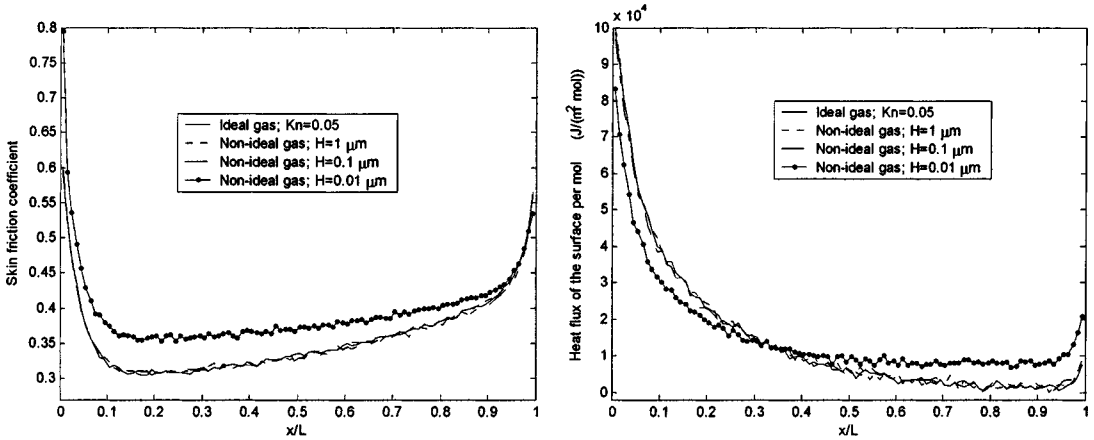

FIG. 4. The skin friction coefficient and the heat transfer flux at the wall surfaces for different channel sizes at Kn=0.05.

tion is satisfied. Therefore, the ideal-gas equation of state holds. This can also be a verification of the CBA modification at a rarefied gas state. However, for the channel having a height of 0.01 μm, the distributions obtained from the two models become rather different. Though the velocity and temperature distributions near the wall are the same as those of an ideal gas, they are much larger far from the wall surfaces. It is also noticed that the density in this case is so high that the ideal-gas assumption breaks down and the nonideal effect must be considered.

Figure 3 presents the velocity and temperature distributions at both the inlet and outlet for different channel sizes at Kn$=0.05$. One interesting finding, similar to the cases (cases 1 and 3), is that the velocity and temperature distributions for the channel having a height of 1 μm simulated by the nonideal-gas model are almost identical to those simulated by the ideal-gas model. In the channels having heights of 0.1 and 0.01 μm, the density is higher than that at atmosphere and the nonideal-gas effect becomes significant. The results for Kn$=0.05$ are different from the cases for Kn$=1.0$ presented in Fig. 2. For example, the inlet temperature at the positions away from the wall surfaces is lower than that obtained by the ideal-gas model for the channel of 0.1 μm in height. The nonideal-gas effect becomes quite large in the channel of 0.01 μm in height, and even the velocity and temperature distributions near the wall become quite different.

A comparison between Figs. 2 and 3 shows that for a given channel size, a low Knudsen number leads to a more significant nonideal-gas effect, such as case 5 and case 6. This may be attributed to the gas density difference. A small Knudsen number will result in a higher gas density, which affects the nonideal-gas effect directly. However, the density is not the only factor that influences the nonideal-gas effect. A comparison between the channel 0.1 μm in height at Kn $=0.05$ (case 4) and the channel 0.01 μm in height at Kn $=1.0$ (case 5) shows that the density of case 4 is higher than that of case 5, however the flow-field distributions of case 5 in the nonideal-gas model are more different from those in the ideal-gas model than case 4. Therefore, the nonideal-gas effect is dependent not only on the density of gas but also on the system size. The smaller the characteristic length, the more important the van der Waals effect.

B. Skin friction and heat transfer of surfaces

The shear stress τ is the sum of the tangential momentum fluxes of both the incident and the reflected molecules at each time step, so the skin friction coefficient is defined as

$$C_f=\frac{\tau}{\frac{1}{2}\rho_\infty u_\infty^2}=\frac{\tau_i+\tau_r}{\frac{1}{2}\rho_\infty u_\infty^2}, \tag{15}$$

where the subscripts "i" and "r" denote the incident and reflected molecular streams, respectively.

The net heat transfer flux q is the sum of the translational and rotational energies of both the incident and the reflected molecules, i.e.,

$$q=\frac{[(\Sigma_{i=1}^{n}\varepsilon_{tr}+\Sigma_{i=1}^{n}\varepsilon_{rot})_i+(\Sigma_{i=1}^{n}\varepsilon_{tr}+\Sigma_{i=1}^{n}\varepsilon_{rot})_r]N_0}{\Delta t(1\cdot\Delta x)}, \tag{16}$$

where n is the total number of simulated molecules that strike the wall during the sampling, N_0 is the number of gaseous molecules associated with a computational molecule, and Δt is the time period of the sampling.

Figure 4 shows the skin friction coefficients and the heat flux per mole for different channel sizes at Kn$=0.05$ (cases 2, 4, and 6). The heat flux is normalized by the mole number of the approaching gas in each case so that different cases can be compared in the same figure. The figure shows that the van der Waals effect affects the resistance and the heat transfer rate at the surfaces when the ideal-gas assumption breaks down. The nonideal-gas effect causes a lower skin friction coefficient along the wall surfaces. The heat transfer flux at the wall obtained by the nonideal-gas model is different from that by the ideal-gas model. Near the inlet the latter is bigger, while near the outlet the former is bigger.

IV. CONCLUSIONS

In micro- and nanoscale gas flow, the gas may be dense due to the very small system characteristic length even though the Knudsen number is high. As a result, the ideal-gas assumption breaks down and the nonideal-gas effect must be considered. The nonideal-gas flow and heat transfer in micro- and nanoscale channels are investigated in the present paper using the modified DSMC method with the consistent Boltzmann algorithm. The van der Waals equation is used as the equation of state by adding a displacement due to the van der Waals force. The collision rate is also modified based on the Enskog theory for dense gases.

The results obtained show that the nonideal-gas effect can be ignored when the gas density is so small that the gas can be treated as a rarefied gas, and that it must be considered when the gas density is high. The nonideal-gas effect leads to different flow-field distributions in the channels. A higher gas density results in a larger difference. However, the gas density is not the only factor that influences the nonideal-gas effect. The channel size also plays a very important role. For a given dense gas, a smaller channel size leads to a more remarkable van der Waals effect. The nonideal-gas effect also causes a lower skin friction coefficient and a different heat transfer flux at wall surfaces.

ACKNOWLEDGMENTS

The present work was supported by the National Natural Science Foundation of China (Grant No. 59995550-2) and National Key Basic Research and Development Program of China (Grant No. 1999033106). The authors would also like to thank J. Fan, T. S. Zhao, and A. L. Garcia.

[1] S. Fukui and R. Kaneko, *Molecular Gas Film Lubrication*, in *Handbook of Micro/Nanotribology*, edited by B. Bhushan (CRC, Boca Raton, FL, 1995).
[2] H.H. Gatzen, Tribol. Int. **33**, 337 (2000).
[3] G.A. Bird, *Molecular Gas Dynamics and the Direct Simulation of Gas Flows* (Clarendon Press, Oxford, 1994); G.A. Bird, *Molecular Gas Dynamics* (Clarendon Press, Oxford, 1976).
[4] G.A. Bird, Comput. Math. Appl. **35**, 1 (1998).
[5] E.S. Oran, C.K. Oh, and B.Z. Cybyk, Annu. Rev. Fluid Mech. **30**, 403 (1998).
[6] C.K. Oh, E.S. Oran, and R.S. Sinkovits, J. Thermophys. Heat Transfer **11**, 497 (1997).
[7] W.W. Liou and Y. Fang, J. Microelectromech. Syst. **10**, 274 (2001).
[8] N.G. Hadjiconstantinou and O. Simek, J. Heat Transfer **124**, 356 (2002).
[9] J. Fan and C. Shen, J. Comput. Phys. **167**, 393 (2001).
[10] Q. Sun and I.D. Boyd, J. Comput. Phys. **179**, 400 (2002).
[11] M.R. Wang and Z.X. Li, Sci. China E (to be published).
[12] D.B. Hash and H.A. Hassan, J. Thermophys. Heat Transfer **8**, 758 (1994).
[13] J. Fan, Phys. Fluids **14**, 4399 (2002).
[14] M.R. Wang and Z.X. Li, Gas Flow and Heat Transfer in Micro/Nano Channels Using DSMC with Different Models, The Fourth International Conference on Fluid Mechanics (to be published).
[15] F.J. Alexander, A.L. Garcia, and B.J. Alder, Phys. Rev. Lett. **74**, 5212 (1995).
[16] N.G. Hadjiconstantinou, A.L. Garcia, and B.J. Alder, Physica A **281**, 337 (2000).
[17] G. Kortemeyer, F. Daffin, and W. Bauer, Phys. Lett. B **374**, 25 (1996).
[18] F.J. Alexander, A.L. Garcia, and B.J. Alder, Physica A **240**, 196 (1997).
[19] J.G. Aston and J.J. Fritz, *Thermodynamics and Statistical Thermodynamics* (Wiley, New York, 1959).
[20] P.P.J.M. Schram, *Kinetic Theory of Gas and Plasmas* (Kluwer Academic Pulishers, Dordrecht, 1991).
[21] A.L. Garcia (private communications); A.L. Garcia, F.J. Alexander, and B.J. Alder, J. Stat. Phys. **89**, 403 (1997); A.L. Garcia and W. Wagner, Transp. Theory Stat. Phys. **31**, 579 (2002).